Combination of UAV and terrestrial photogrammetry to assess rapid glacier evolution and map glacier hazards

Fugazza, Davide[1]; Scaioni, Marco[2]; Corti, Manuel[2]; D'Agata, Carlo[3]; Azzoni, Roberto Sergio[3]; Cernuschi, Massimo[4]; Smiraglia, Claudio[1]; Diolaiuti, Guglielmina Adele[3]

[1]Department of Earth Sciences 'A.Desio', Università degli studi di Milano, 20133 Milano Italy

[2]Department of Architecture, Built Environment and Construction Engineering, Politecnico di Milano, 20133 Milano Italy

[3]Department of Environmental science and policy (DESP), Università degli studi di Milano, 20133 Milano Italy

[4]Agricola 2000 S.C.P.A., 20067 Tribiano (MI) Italy

Correspondence to: Marco Scaioni (marco.scaioni@polimi.it)

Abstract

Tourists and hikers visiting glaciers all year round face hazards such as sudden terminus collapses, typical of such a dynamically evolving environment. In this study, we analysed the potential of different survey techniques to analyse hazards of the Forni glacier, an important geosite located in Stelvio Park (Italian Alps). We carried out surveys in the 2016 ablation season and compared point clouds generated from an unmanned aerial vehicle (UAV) survey, close range photogrammetry and terrestrial laser scanning (TLS). To investigate the evolution of glacier hazards and evaluate the glacier thinning rate, we also used UAV data collected in 2014 and a digital elevation model (DEM) created from an aerial photogrammetric survey of 2007. We found that the integration between terrestrial and UAV photogrammetry is ideal for mapping hazards related to the glacier collapse, while TLS is affected by occlusions and is logistically complex in glacial terrain. Photogrammetric techniques can therefore replace TLS for glacier studies and UAV-based DEMs hold potential for becoming a standard tool in the investigation of glacier thickness changes. Based on our datasets, an increase in the size of collapses was found over the study period, and the glacier thinning rates went from 4.55 ± 0.24 ma^{-1} between 2007 and 2014 to 5.20 ± 1.11 ma^{-1} between 2014 and 2016.

1 Introduction

Glacier and permafrost-related hazards can be a serious threat to humans and infrastructure in high mountain regions (Carey et al., 2014). The most catastrophic cryospheric hazards are generally related to water outbursts , either through breaching of moraine- or ice-dammed lakes or from the englacial or subglacial system, causing floods and debris flows. Ice avalanches from hanging glaciers can also have serious consequences for downstream populations (Vincent et al., 2015), as well as debris flows caused by the mobilization of accumulated loose sediment on steep slopes (Kaab et al., 2005a). Less severe hazards, but still particularly threatening for mountaineers, are the detachment of seracs

(Riccardi et al., 2010) or the collapse of ice cavities (Gagliardini et al., 2011; Azzoni et al., 2017). While these processes are in part typical of glacial and periglacial environments, there is evidence that climate change is increasing the likelihood of specific hazards (Kaab et al., 2005a). In the European Alps, accelerated formation and growth of proglacial moraine-dammed lakes has been reported in Switzerland, amongst concern of possible overtopping of moraine dams provoked by ice avalanches (Gobiet et al., 2014). Ice avalanches themselves can be more frequent as basal sliding is enhanced by the abundance of meltwater in warmer summers (Clague, 2013). Glacier and permafrost retreat, which have been reported in all sectors of the Alps (Smiraglia et al., 2015; Fischer et al., 2014; Gardent et al., 2014; Harris et al., 2009), are a major cause of slope instabilities which can result in debris flows, by debuttressing rock and debris flanks and promoting the exposure of unconsolidated and ice-cored sediments (Keiler et al., 2010; Chiarle et al., 2007). Glacier downwasting causes changes in water resources, with an initial increase in discharge due to enhanced melt followed by a long-term reduction, affecting drinking water supply, irrigation and hydropower production (Kaab et al., 2005b), along with a rising occurrence of structural collapses (Azzoni et al., 2017). Finally, glacier retreat and the increase in glacier hazards both negatively influence the tourism sector and the economic prosperity of high mountain regions (Palomo, 2017).

The growing threat from cryospheric hazards under climate change calls for the adoption of mitigation strategies. Remote sensing has long been recognized as an important tool for producing supporting data for this purpose, such as digital elevation models (DEMs) and multispectral images. DEMs are particularly useful for detecting glacier thickness and volume variations (Fischer et al., 2015; Berthier et al., 2016) and for identifying steep areas that are most prone to geomorphodynamic changes, such as mass movements (Blasone et al., 2014). Multispectral images at a sufficient spatial resolution make it possible to recognize most cryospheric hazards (Quincey et al., 2005; Kaab et al., 2005b). While satellite images from Landsat and ASTER sensors (15-30 m ground sample distance - GSD) are practical for regional-scale mapping (Rounce et al, 2017), the assessment of hazards at the

scale of individual glaciers or basins requires a higher spatial resolution, which in the past could only be achieved via aerial laser scanner/photogrammetric surveys (Vincent et al., 2010; Janke, 2013) or dedicated field campaigns with terrestrial laser scanners (TLS) (Kellerer-Pirklbauer et al., 2005; Riccardi et al., 2010). Recent years have seen a resurgence of terrestrial photogrammetric surveys for the generation of DEMs (Piermattei et al., 2015, 2016; Kaufmann and Seier, 2016) due to important technological advances, including the development of Structure-from-Motion (SfM) photogrammetry and its implementation in fully automatic processing software, as well as improvements in the quality of camera sensors (Eltner et al., 2016; Westoby et al., 2012). In parallel, unmanned aerial vehicles (UAVs – Colomina & Molina, 2014, O'Connor et al., 2017) have started to emerge as a viable alternative to TLS for multi-temporal monitoring of small areas. UAVs promise to bridge the gap between field observations, notoriously difficult on glaciers, and coarser resolution satellite data (Bhardwaj et al., 2016). Although the number of studies employing these platforms in high mountain environments is on the rise (see e.g. Fugazza et al., 2015; Gindraux et al., 2017; Seier et al., 2017), their full potential for monitoring glaciers and particularly glacier hazards has yet to be explored. In particular, the advantages of UAV and terrestrial SfM-photogrammetry and the possibility of data fusion and volume change estimation to support hazard management strategies in glacial environments needs to be investigated and assessed.

In this study, we investigated a rapidly downwasting glacier (almost 5 ma^{-1} water equivalent, Senese et al., 2012) in a protected area and highly touristic sector of the Italian Alps, Stelvio National Park. We focused on the glacier terminus and the hazards identified there, i.e., the formation of normal faults and ring faults. The former occur mainly on the medial moraines and glacier terminus and are due to gravitational collapse of debris-laden slopes. The latter develop as a series of circular or semicircular fractures with stepwise subsidence, caused by englacial or subglacial meltwater creating voids at the ice-bedrock interface, eventually leading to the collapse of the cavity roofs. While often overlooked, these collapse structures are particularly hazardous for mountaineers and they are likely to increase under a

85 climate change scenario (Azzoni et al., 2017). They are more dangerous than crevasses because of their
86 larger size.

87 We conducted our first UAV survey of the glacier in 2014; in summer 2016, the glacier was surveyed
88 using three different techniques for the generation of point clouds, DEMs and orthophotos. The aims
89 were: (1) to compare the different methods and select the most appropriate ones for monitoring glacier
90 hazards (2) to identify glacier-related hazards and their evolution between 2014-2016; and 3) to
91 investigate changes in ice thickness between 2014-2016 and 2007-2016 by comparing the two UAV
92 DEMs and a third DEM obtained from stereo-processing of aerial photos captured in 2007.

93

94 **2 Study area**

95 The Forni Glacier (see Fig. 1) has an area of 11.34 km^2 based on the 2007 data from the Italian Glacier
96 Inventory (Smiraglia et al., 2015); an altitudinal range between 2501 and 3673 m a.s.l., and a North-
97 North-Westerly aspect. The glacier has retreated markedly since the little ice age, when its area was
98 17.80 km^2 (Diolaiuti & Smiraglia, 2010), with an acceleration of the shrinkage rate over the past three
99 decades, typical of valley glaciers in the Alps (Diolaiuti et al., 2012, D'Agata et al.; 2014). It has also
100 undergone profound changes in dynamics in recent years, such as the loss of ice flow from the eastern
101 accumulation basin towards its tongue and the evidence of collapsing areas on the eastern tongue (see
102 Fig. 2d; Azzoni et al., 2017). Continuous monitoring of these hazards is important, as the site is highly
103 touristic (Garavaglia et al., 2012). The glacier is in fact frequently visited during both summer and
104 winter months. During the summer, hikers heading to Mount San Matteo take the trail along the
105 central tongue, accessing the glacier through the left flank of the collapsing glacier terminus (see Fig.
106 2b, c). During wintertime, ski-mountaineers instead access the glacier from the eastern side, crossing
107 the medial moraine and potentially collapsed areas there (see Fig. 1, 2a).

108 **3 Data sources: acquisition and processing**

In this study, we took advantage of a UAV survey performed in 2014 (Fugazza et al., 2015). Then, through a field campaign in 2016, we conducted different surveys using a UAV, terrestrial photogrammetry and TLS. In the 2014 UAV survey, no ground control points (GCPs) were collected, while in 2016 we specifically set up a control network for geo-referencing purposes. Processing of the UAV and terrestrial images was carried out using Agisoft Photoscan version 1.2.4 (www.agisoft.com), implementing a SfM algorithm for image orientation followed by a multi-view dense-matching approach for surface 3D reconstruction (Westoby et al., 2012). In addition, we employed a DEM from an aerial survey of 2007 to calculate glacier thickness changes over a period of 7 to 9 years.

3.1 UAV photogrammetry

3.1.1 2014 Dataset

The first UAV survey took place on 28th August 2014, using a SwingletCam fixed wing aircraft (see Fig. 3a). This commercial platform developed by SenseFly carries a Canon Ixus 127 HS compact digital camera. The UAV was flown in autopilot mode with a relative flying height of approximately 380 m above the glacier surface, which resulted in an average GSD of 12 cm. The flight plan was organized by using the proprietary software eMotion, by which the aircraft follows predefined waypoints with a nominal along-strip overlap of 70%. In our study, sidelap was not regular because of the varying surface topography, but it averaged approximately 60%. Flight operations started around 07:30 AM and ended around 08:30 AM. Early morning operations were preferred to avoid saturating camera pictures, as during this time of day the glacier is not yet directly illuminated by the sun, and to minimize blurring effects due to the UAV motion, since wind speed is at its lowest on glaciers during morning hours (Fugazza et al., 2015). Pictures were automatically captured by the UAV platform, selecting the best combination of sensor aperture (F=2.7), sensitivity (between 100-400 ISO) and shutter speed (between 1/125 s - 1/640 s). The survey covered an area of 2.21 km^2 in

two flight campaigns, with a low altitude take-off (see Fig. 1). Both the terminal parts of the central and eastern ablation tongue were surveyed.

Since no GCPs were measured during the 2014 campaign, the registration of this data set into the mapping reference system was based on GNSS (Global Navigation Satellite System) navigation data only. Consequently, a global bias in the order of 1.5-2 m resulted after geo-referencing, and no control on the intrinsic geometric block stability was possible. After the generation of the point cloud, a DEM and orthophoto were produced with spatial resolutions of 60 cm and 15 cm, respectively.

3.1.2 2016 Dataset

Two UAV surveys were carried out on 30th August and 1st September 2016, both around midday with 8/8 of the sky covered by stratocumulus clouds. The UAV employed in these surveys was a customized quadcopter (see Fig. 3b) carrying a Canon Powershot 16 Megapixel digital camera. Two different take-off and landing sites were chosen to gain altitude before take-off and maintain line-of-sight operation with a flying altitude of 50 m above ground, which ensured an average ground sample distance (GSD) of 6 cm. To reduce motion blur, camera shutter speed was set to the lowest possible setting, 1/2000 s, with aperture at F/2.7 and sensitivity at 200 ISO.

Several flights were conducted to cover a small section of the proglacial plain and different surface types on the glacier surface, including the terminus, a collapsed area on the central tongue, the eastern medial moraine and some debris-covered parts of the eastern tongue. A ‘zig-zag’ flying scheme was followed to reduce the flight time. The UAV was flown in autopilot mode using the open-source software Mission Planner (Oborne, 2013) to ensure 70% along-strip overlap and sidelap. In total, two flights were performed during the first survey and three during the second, lasting about 20 minutes each. The surveyed area spanned over 0.59 km^2.

Eight GCPs (see Fig. 1) were measured for the registration of the photogrammetric blocks and its by-products into the mapping system. The root mean square error (RMSE) of the GCP location was 40

157 cm, which can be used as an indicator of the internal consistency of the photogrammetric block. The
158 point cloud obtained from the 2016 UAV flight was interpolated to produce a DEM and orthophoto
159 with the same cell resolution as the 2014 dataset, i.e., 60 and 15 cm, respectively. Both products were
160 exported in the ITRS2000 / UTM 32N mapping reference system.

161 **3.2 Terrestrial photogrammetry**

162 The terrestrial photogrammetric survey was carried out on 29th August 2016 to reconstruct the
163 topographic surface of the glacier terminus, which presented several vertical and subvertical surfaces
164 (see Fig. 2e) whose measurement was not possible from the UAV platform carrying a camera in nadir
165 configuration.

166 Images were captured from 134 ground-based stations, most of them located in front of the glacier,
167 and some on both flanks of the valley in the downstream area. A single-lens-reflex Nikon D700
168 camera was used, equipped with a 50 mm lens, and a full-frame CMOS sensor (36x24 mm) with
169 4256x2823 pixels. In this case, since no preliminary information about approximate camera position
170 was collected, the SfM procedure was run without any initial information.

171 Seven natural features visible on the glacier front were used as GCPs to be included in the bundle
172 adjustment computation. Measurement of GCPs in the field was carried out by means of a high-
173 precision theodolite. The measurement of points previously recorded with a GNSS geodetic receiver
174 made it possible to register the coordinates of GCPs in the mapping reference system. The RMSE of
175 3D residual vectors on GCPs was 34 cm.

176 **3.3 Terrestrial Laser Scanning**

177 On the same days as the first UAV survey of 2016, a long-range terrestrial laser scanner Riegl LMS-
178 Z420i was used to scan the glacier terminus. One instrumental standpoint located on the hydrographic
179 left flank of the glacier terminus (see Fig. 1) was established. The horizontal and vertical scanning

180 resolution were set up to provide a spatial point density of approx. 5 cm on the ice surface at the
181 terminus. Geo-referencing was accomplished by placing five GCPs consisting in cylinders covered
182 by retroreflective paper. The coordinates of GCPs were measured by using a precision theodolite
183 following the same procedure adopted for terrestrial photogrammetry. Considering the accuracy of
184 registration and the expected precision of laser point measurement, the global uncertainty of 3D points
185 was estimated on the order of ±7.5 cm.

186 **3.4 GNSS ground control points**

187 Prior to the 2016 surveys, eight control targets were placed both on the periglacial area and on the
188 glacier tongue (see Fig. 1). Differential GNSS (global navigation satellite system) data were acquired
189 at the target location for the geo-referencing of UAV, terrestrial photogrammetry and TLS data. GCPs
190 were used 1) to geo-reference UAV data directly, by identifying the targets on the images in
191 Photoscan; 2) to register theodolite measurements for geo-referencing terrestrial photogrammetry and
192 TLS. The targets consisted in a square piece of white fabric (80 x 80 cm), with a circular marker in
193 red paint chosen to provide contrast against the background. Except for the one GCP located at the
194 highest site, such GCPs were positioned on large, flat boulders to provide a stable support and reduce
195 the impact of ice ablation between flights.

196 GNSS data were acquired by means of a pair of Leica Geosystems 1200 geodetic receivers working
197 in RTK (Real-Time Kinematics) mode (see Hoffman-Wellenhof, 2008). One of them was set up as
198 master on a precise point beside Branca hut, with known coordinates in the mapping reference system
199 ITRS2000 / UTM 32N. The second receiver was used as a rover, communicating via radio link with
200 the master station. The maximum distance between master and rover was less than 1.5 km, but due
201 to the local topography preventing the radio link and the lack of mobile phone services (for RTK),
202 some points were measured in static mode with measurement time of approximately 12 minutes. The
203 theoretical uncertainty of GCPs provided by the processing code was on the order of 2-3 cm.

3.5 2007 DEM

The 2007 TerraItaly DEM was produced by the BLOM C.G.R. company for the Lombardy region. It is the final product of an aerial survey over the entire region, conducted with a multispectral pushbroom Leica ADS40 sensor acquiring images from a flying height of 6,300 m with an average GSD of 65 cm. The images were processed to generate a DEM with a cell resolution of 2 m x 2 m, and a ±3 m uncertainty. We converted the DEM from the "Monte Mario" to the "ITRS2000" datum and the height from ellipsoidal to geodetic using the official software for datum transformation in Italy (Verto ver. 3).

4 Methods

4.1 Analysis of point clouds from the 2016 campaign: UAV/terrestrial photogrammetry and TLS

The comparison between point clouds generated during the 2016 campaign had the aim of assessing their geometric quality before their application for the analysis of hazards. These evaluations were also expected to provide some guidelines for the organization of future investigations in the field at the Forni Glacier and in other Alpine sites. Specifically, we analysed point density (points/m^2) and completeness, i.e. % of area in the ray view angle. Point density partly depends upon the surveying technique used, since it is controlled by the distance between sensor and surface, and determines spatial resolution. In SfM-photogrammetry, point density is affected by image texture, sharpness and resolution, which influence the performance of dense matching algorithms (Dall'Asta et al., 2015), while in TLS it can be set up as a data acquisition input parameter. In this study, the number of neighbours N (inside a sphere of radius R=1 meter) divided by the neighbourhood surface was used to evaluate the local point density D in CloudCompare (www.cloudcompare.org). To understand the effect of point density dispersion (Teunissen, 2009), the inferior 12.5 percentile of the standard deviation σ of point density was also calculated. The use of these local metrics allowed us to distinguish between point densities in different areas, since this may largely change from one portion

of surface to another. A further metric in this sense was point cloud completeness, referring to the presence of enough points to completely describe a portion of surface. In this study, the visual inspection of selected sample locations was used to identify occlusions and areas with lower point density.

To analyse these properties, five regions were selected (see Fig. 4), located on the glacier topographic surface and characterized by different glacier features and the presence of hazards: 1) a glacial cavity composed of subvertical and fractured surfaces over 20 m high, and forming a typical semicircular shape; 2) a glacial cavity over 10 m high with the same typical semi-circular shape as location 1, covered by fine- and medium-sized rock debris; 3) a normal fault over 10 m high; 4) a highly-collapsed area covered by fine- and medium-sized rock debris and rock boulders; and 5) a planar surface with a normal fault covered by fine- and medium-sized rock debris and rock boulders. The analysis of local regions was preferred to the overall analysis of all the point clouds for the following reasons: 1) the incomplete overlap between point clouds obtained from different methods; 2) the opportunity to investigate the performances of the techniques in diverse geomorphological situations.

Within the same sample locations, we compared the point clouds in a pairwise manner. Since no available benchmarking data set (e.g. accurate static GNSS data) was concurrently collected during the 2016 campaign, the TLS point cloud was used as a reference. When comparing both photogrammetric data sets, the one obtained from the UAV was used as reference because of the even distribution of point density within the sample locations. The presence of residual, non-homogenous geo-referencing errors in the data sets required a specific fine registration of each individual sample location, which was conducted in CloudCompare using the ICP (iterative closest point) algorithm (Pomerleau et al., 2013). ICP iteratively matches a source point cloud to a reference point cloud in Euclidean space and calculates the necessary rotation and translation to align the source point cloud with the reference based on minimization of a distance metric in a point-to-point fashion. After fine registration, point clouds in corresponding sample areas were compared using the M3C2 algorithm

implemented in CloudCompare (Lague et al., 2013). As discussed in Fey and Wichmann (2016), the distance between a pair of point clouds is often evaluated by comparing elevations at corresponding nodes of DEMs, after resampling of the original data. This approach works properly when both point clouds are approximately aligned along the same planar direction, but not when there are structures with different alignments as in the case of the glacier surfaces under investigation. In fact, the M3C2 algorithm does not always evaluate the distance between two point clouds along the same directional axis, but computes a set of local normals using points within a radius D depending on the local roughness, which is directly estimated from the point cloud data, and also considering the accuracy of preliminary local registration refinement using ICP. In this case, a radius D=20 cm and a pre-registration accuracy of 5 cm were considered, the latter obtained from ICP residuals. This solution allowed us to remove registration errors from the analysis, and focus on the capability of the adopted techniques to reconstruct the local geometric surface of the glacier in an accurate way.

4.2 Point cloud merging

To improve coverage of different glacier surfaces, including planar areas and normal faults, photogrammetric point clouds from the 2016 campaign (UAV and terrestrial surveys) were merged. We chose to avoid TLS and employed the two lower cost techniques (Chandler and Buckley, 2016) to assess their potential for combined future use. Prior to point cloud merging, a preliminary co-registration was performed on the basis of the ICP algorithm in CloudCompare. Regions common to both point clouds were used to minimize the distances between them and find the best co-registration. The point cloud from UAV photogrammetry, which featured the largest extension, was used as reference during co-registration, while the other was rigidly transformed to fit with it. After many iterations, both point clouds were aligned according to the best solution found by the ICP. In order to remove redundant points and to obtain a homogenous point density, the merged point cloud (see Fig. 5) was subsampled keeping a minimum distance between adjacent points of 20 cm. The final size of this merged data set is approximately 4.4 million points. The RGB colour information associated with

each point in the final point cloud was derived by averaging the RGB information of original points in the subsampling volumes. While this operation resulted in losing part of the original RGB information, it helped to provide a realistic visualization of the topographic model, and therefore to interpret glacier hazards.

4.2 Glacier hazard mapping

The investigation of glacier hazards was conducted using the point cloud and orthophoto from the 2014 UAV dataset as well as the merged (UAV and terrestrial) point cloud and orthophoto from 2016. In this study, we focused on ring faults and normal faults, which were identified by visually inspecting their geometric properties in the point clouds and manually delineated, while colour information from orthophotos was used as a cross-check. On orthophotos, both types of structures generally appear as dark linear features owing to shadows projected by fault scarps. As these structures may look similar to crevasses, further information concerning their orientation and location needs to be assessed for discrimination. The orientation of fault structures is not coherent with glacier flow, with ring faults also appearing in circular patterns. Their location is limited to the glacier margins, medial moraines and terminus, whereas crevasses can appear anywhere on the glacier surface (Azzoni et al., 2017). After delineation, we also analysed the height of vertical facies using information from the point clouds.

4.3 DEM Co-registration for glacier thickness change estimation

Several studies have found that errors in individual DEMs, both in the horizontal and vertical domain, propagate when calculating their difference, leading to inaccurate estimations of thickness and volume change (Berthier et al., 2007; Nuth & Kaab, 2011). In the present study, different approaches were adopted for geo-referencing all the DEMs used in the analysis of the volume change of the Forni Glacier tongue (2007, 2014, 2016). To compute the relative differences between the DEMs, a preliminary co-registration was therefore required. The method proposed by Berthier et al. (2007) for

303 the co-registration of two DEMS was separately applied to each DEM pair (2007-2014; 2007-2016;
304 2014-2016). Following this method, in each pair one DEM plays as reference ('master'), while the
305 other is used as 'slave' DEM to be iteratively shifted along x and y axes by fractions of a pixel to
306 minimize the standard deviation of elevation differences with respect to the 'master' DEM. Only areas
307 assumed to be stable are considered in the calculation of the co-registration shift. The ice-covered
308 areas were excluded by overlaying the glacier outlines from D'Agata et al. (2014) for 2007 and
309 Fugazza et al. (2015) for 2014. The oldest DEM, which is also the widest in each comparison, was
310 always set as the master. To co-register the 2014 and 2016 DEMs with the 2007 DEM, both were
311 resampled to 2 m spatial resolution, whereas the comparison between 2014 and 2016 was carried out
312 at the original resolution of these data sets (60 cm).

313 All points resulting in elevation differences greater than 15 m were labelled as unreliable, and
314 consequently discarded from the subsequent analysis. Such greater discrepancies may denote errors
315 in one of the DEMs or unstable areas outside the glacier. Values exceeding this threshold, however,
316 were only found in a marginal area with low image overlap in the comparison between the 2014 and
317 2016 DEMs, with a maximum elevation difference of 36 m. Once the final co-registration shifts were
318 computed (see Table 1), the coefficients were subtracted from the top left coordinates of the 'slave'
319 DEM; the residual mean elevation difference was also subtracted from the 'slave' DEM to bring the
320 mean to zero. After DEM co-registration, the resulting shifts reported in Table 1 were applied to each
321 'slave' DEM, including the entire glacier area. Then the elevations of the 'slave' DEM were subtracted
322 from the corresponding elevations of the 'master' DEM to obtain the so- called DEM of Differences
323 (DoD). Over a common glacier area (Fig. 1), we estimated the volume change and its uncertainty,
324 which can be expressed as the combination of 1) uncertainty due to errors in elevation and 2) the
325 truncation error caused by the use of a discrete sum (sum of DoD at each pixel multiplied by pixel
326 area) in place of the integral in volume calculation (Jokinen and Geist, 2010). We calculated the
327 former following the approach of Rolstad et al. (2009), taking into account spatial autocorrelation of

328 elevation change over stable areas, considering a correlation length of 50 m; for the latter, we used
329 the method described by Jokinen and Geist (2010).

330 **5 Results**

331 **5.1 Point cloud Analysis**

332 The analysis of point density shows significant differences between the three techniques for point
333 cloud generation (see Table 2). Values range from 103 to 2297 points/m^2 depending on the surveying
334 method, but the density was generally sufficient for the reconstruction of the different surfaces shown
335 in Fig. 4, except for location 5. Terrestrial photogrammetry featured the highest point density, while
336 UAV photogrammetry had the lowest. In relation to UAV photogrammetry, similar point densities
337 were found in all sample locations, especially for the standard deviations that were always in the 22-
338 29 point/m^2 range. Mean values were 103-109 points/m^2 in locations 2-4, while they were higher in
339 location 5 (141 points/m^2). Due to the nadir acquisition points, the 3D modelling of vertical/sub-
340 vertical cliffs in location 1 was not possible. In relation to TLS, a mean value of point density ranging
341 from 141-391 points/m^2 was found, with the only exception of location 5, where no sufficient data
342 were recorded due to the position of this region with respect to the instrumental standpoint. Standard
343 deviations ranged between 69-217 points/m^2, moderately correlated with respective mean values. The
344 analysis of the completeness of surface reconstruction also revealed some issues related to the adopted
345 techniques (see Fig. 5). Specifically, TLS suffered from severe occlusions, which prevented
346 acquisition of data in the central part of the sample area, while UAV photogrammetry was able to
347 reconstruct the upper portion of the sample area but not the vertical cliff. Only terrestrial
348 photogrammetry acquired a large number of points in all areas.

349 In terms of point cloud distance (see Table 3), the comparison between TLS and terrestrial
350 photogrammetry resulted in a high similarity between point clouds, with no great differences between
351 different sample areas. Conversely, the comparison between TLS and UAV photogrammetry and
352 terrestrial and UAV photogrammetry provided significantly worse results, which may be summarized

by the RMSEs in the range 21.1-37.7 cm and 20.7-30.4 cm, respectively. The greater deviations were in both cases obtained in the analysis of location 2, which mostly represents a vertical surface, while the best agreement was found within location 3 which is less inclined. As the UAV flight was geo-referenced on a set of GCPs with an RMSE of 40.5 cm, the ICP co-registration may have not totally compensated the existing bias.

In terms of spatial coverage, considering the entire surface examined using each technique outside the sample locations, the UAV survey extended over the widest area (0.59 km^2), including part of the proglacial plain, the entire terminus and the glacier tongue up to the collapsed area on the central part, but with data gaps on the vertical and sub-vertical walls (see Fig. 6a). The point cloud obtained from terrestrial photogrammetry covered approximately a third of the area surveyed with the UAV (see fig. 6b), including the full glacier terminus at very high spatial resolution, with the exception of a few obstructed parts, while the TLS point cloud covered the terminus, although with some holes due to the obstructions.

5.2 Glacier-related hazards and risks

The tongue of Forni glacier hosts several hazardous structures, including crevasses, normal faults and ring faults. In this study, we focused on the latter two due to their relationship with glacier downwasting. While most collapsed areas on Forni glacier are normal faults, two large ring fault systems can be identified: the first, located in the eastern section (see Fig. 2d and Fig. 7), covered an area of 25.6×10^3 m^2 and showed surface dips of up to 5 m in 2014. This area was not surveyed in 2016, since field observation did not show evidence of further significant subsidence. Conversely, the ring fault that only emerged as a few semi-circular fractures in 2014 grew until cavity collapse, with a vertical displacement up to 20 m. Additional fractures, extending south-eastward (see Fig. 2c and Fig. 7), formed between 2014 and 2016, suggesting that the extent of the collapse might widen in the near future. In 2014, further ring faults were also identified at the eastern glacier margin, and the one

377 that was surveyed in 2016 showed evidence of increasing subsidence (+2 m) and the formation of
378 additional subparallel fractures.

379 Normal faults are mostly found on the eastern medial moraine and at the terminus. Between 2014 and
380 2016, the first (see Fig. 2a) developed rapidly in the vertical domain reaching a height of 12 m in
381 2016. The latter increased in number as size, as the terminus underwent collapse, leading to the
382 formation of three major ice cavities, up to 24 m high (see Fig. 2b and 2e). In 2016, ice thickness
383 above the cavity vault was between 5 and 10 m (see Fig. 4, location 1). Several fractures identified
384 as normal faults also appear in conjunction with the large ring fault located in the central section of
385 the glacier, extending the fracture system to the western glacier margin.

386 The presence of cavities at the terminus, which is easily reached in a 45 minutes' walk from Branca
387 hut, is particularly hazardous for tourists, because of 1) the danger of cavity collapse and 2) the
388 potential fall of large boulders or blocks of ice from the ice cliffs. Other fracture systems located
389 higher up glacier are presumably reached by more experienced hikers. Most ring faults however show
390 evidence of vertical and horizontal expansion, and further cavity collapse would imply a severe risk
391 of injury and death if hikers were involved.

392 The location of structures in 2016 suggests that the glacier terminus will recede through ice cliff
393 backwasting and cavity collapse along the fault system on the eastern medial moraine and along the
394 ring faults at the eastern and western margins, potentially compromising access to the glacier. Since
395 this system of fractures has been developing very rapidly, and new collapses have already been
396 documented in September 2017, the risk for people walking on the glacier tongue during summer
397 should be carefully evaluated. Although surface features may be visually detected, the availability of
398 detailed 3D models that depict the entire outer surface of the glacier is a great advantage because it
399 allows quickly capturing the glacier topography remotely, helping predict the possible development
400 of new collapses and understand their mechanisms of formation.

401 **5.3 Glacier thickness change**

402 The Forni Glacier tongue was affected by substantial thinning throughout the observation period.
403 Between 2007 and 2014, the greatest thinning occurred in the eastern section of the glacier tongue,
404 with changes persistently lower than –30 m (more than 4 ma^{-1} thinning), whereas the upper part of
405 the central tongue only thinned by 10/18 m (between approximately 1 and 2.5 ma^{-1}). The greatest ice
406 loss occurred in correspondence with the normal faults localized in small areas at the eastern glacier
407 margin (see Fig. 8a), with local changes generally lower than -50 m (more than 7 ma^{-1} thinning) and
408 a minimum of -66.80 m, owing to the formation of a lake. Conversely, between 2014 and 2016 the
409 central and eastern parts of the tongue had similar thinning patterns, with average changes of -10 m
410 (5 ma^{-1}). The greatest losses are mainly found in correspondence with normal faults, with a maximum
411 change of -38.71 m at the terminus and local thinning greater than 25 m on the lower medial moraine.
412 The ring fault at the left margin of the central section of the tongue also shows thinning of 20 to 26
413 m (10-13 ma^{-1}). In the absence of faults, little thinning occurred instead on the upper part of the medial
414 moraine, where a thick debris cover shielded ice from ablation, with changes of -2 to -5 m (1 to 2.5
415 ma^{-1}, see Fig. 8c). Considering a common reference area (see Fig. 1, table 4), an acceleration of glacier
416 thinning seems to have occurred over recent years over the lower glacier tongue, from -4.55 ± 0.24
417 ma^{-1} in 2007-2014 to -5.20 ± 1.11 ma^{-1} in 2014-2016, also confirmed by the value of -4.76 ± 0.29 ma^{-1}
418 obtained from the comparison between 2007 and 2016. Looking at the first two DoD, the trend
419 seems to be caused by the increase in collapsing areas (Fig.8a,b). In all DoDs, the uncertainty in ice
420 thickness change affects less than 3% of the respective volume change (see Table 4).

421

422 **6 Discussion: comparison of techniques for point cloud generation**

423 The choice of a technique to monitor glacier hazards and the glacier thickness changes depends on
424 several factors, including the size of the area, the desired spatial resolution and accuracy, logistics

425 and cost. In this study, we focused on spatial metrics, i.e. point density, completeness and distance
426 between point clouds to evaluate the performance of UAV, close-range photogrammetry and TLS in
427 a variety of conditions.

428 **6.1 Point density and completeness**

429 Considering point density, terrestrial photogrammetry resulted in a denser data set than the other
430 techniques. This is mostly motivated by the possibility of acquiring data from several stations using
431 this methodology, depending only on the terrain accessibility, reducing the effect of occlusions with
432 a consequently more complete 3D modelling. However, the mean point density achieved when using
433 terrestrial photogrammetry is highly variable, both between different sample locations, and within
434 each location as shown by the standard deviations of *D*. Point densities related to UAV
435 photogrammetry and TLS are more regular and constant. In the case of UAV photogrammetry, the
436 homogeneity of point density might be due to the regular structure of the airborne photogrammetric
437 block. In the case of TLS, the regularity is motivated by the constant angular resolution adopted
438 during scanning. Since any technique may perform better when the surface to survey is approximately
439 orthogonal to the sensor's point of view, terrestrial photogrammetry is more efficient for
440 reconstructing vertical and subvertical cliffs (Sample areas 1 and 2) and high-sloped surfaces (Sample
441 areas 3 and 4). On the contrary, airborne UAV photogrammetry provided the best results in location
442 5 which is less inclined and consequently could be well depicted in vertical photos. In general, point
443 clouds from terrestrial photogrammetry provide a better description of the vertical and subvertical
444 parts (see e.g. Winkler et al., 2012), while point clouds obtained from UAV photogrammetry are more
445 suitable to describe the horizontal or sub-horizontal surfaces on the glacier tongue and periglacial
446 area (Seier et al., 2017), unless the camera is tilted to an off-nadir viewpoint (Dewez et al., 2016;
447 Aicardi et al., 2016). Results obtained from photogrammetry based on terrestrial and UAV platforms
448 can thus be considered quite complementary and they support the concept of merging the point clouds
449 from these two techniques, as seen in Fig. 6c. In agreement with other studies of vertical rock slopes

(e.g. Abellan et al., 2014), we found that the TLS point cloud was affected by occlusions (see e.g. location 2 in Fig. 4, 5), which can only be compensated by increasing the number of stations. Data acquisition with this platform was in general difficult in regions subparallel to the laser beams and in the presence of wet surfaces.

6.2 Point cloud and DEM uncertainty

In this study, the distance between the UAV and TLS point clouds (21.1-37.7 cm RMSE), assumed as a measure of the uncertainty of the 2016 UAV dataset, was slightly higher than previously reported in high mountain glacial environments (e.g. Immerzeel et al., 2014; Gindraux et al., 2017 and Seier et al., 2017), although in these studies the comparison was between DEMs and GNSS control points. Contributing factors might include the sub-optimal distribution and density of GCPs (Gindraux et al., 2017), the delay between the UAV surveys as well as between the UAV and TLS, and the lack of coincidence between GCP placement and the UAV flights. This means the UAV photogrammetric reconstruction was affected by ice ablation and glacier flow, which on Forni Glacier range between 3 and 5 cm day^{-1} (Senese et al., 2012) and 1-4 cm day^{-1}, respectively (Urbini et al., 2017). We thus expect a combined 3-day uncertainty on the 2016 UAV dataset between 10 and 20 cm, and lower on GCPs considering reduced ablation owing to their placement on boulders. A further contribution to the GCP error budget might stem from the intrinsic precision of GNSS/theodolite measurements and image resolution. The comparison between close-range photogrammetry and TLS was less affected by glacier change as data were collected one day apart and the RMSE of 6-10.6 cm is in line with previous findings by Kaufmann and Landstaedter (2008). To reduce the uncertainty of UAV photogrammetric blocks, a better distribution of GCPs or switching to an RTK system should be considered, while close-range photogrammetry could benefit from measuring a part of the photo-stations as proposed in Forlani et al. (2014), instead of placing GCPs on the glacier surface.

The uncertainty in UAV photogrammetric reconstruction also factored in the standard deviation still present after the co-registration between DEMs in areas outside the glacier (2.22 m between 2014 and 2016). Another important factor here is the morphology of the co-registration area, i.e. the outwash plain, still subject to changes owing to the inflow of glacier meltwater and sediment reworking. UAV photogrammetric products permitted us to investigate ice volume changes over 2 years with an uncertainty of 2.60%, while the integration with close-range photogrammetry was required to investigate hazards related to the collapse of the glacier terminus.

6.3 Logistics and costs

In our surveys, it became evident that the main disadvantage of TLS compared to photogrammetry is the complexity of instrument transport and setup. In terms of logistics and workload, up to five people were involved in the transportation of the TLS instruments (laser scanner, theodolite, at least two topographic tripods and poles, electric generator and ancillary accessories) while two people were required for UAV and close-range photogrammetric surveys, which were also considerably faster. Meteorological conditions and the limited access to unstable areas close to the glacier terminus also prevented the acquisition of TLS data from other viewpoints as done with photogrammetry. Concerning UAV surveys, we conducted them under different meteorological scenarios, and obtained adequate results in early-morning operations with 0/8 cloud cover and midday flights with 8/8 cloud cover. Both scenarios can provide diffuse light conditions allowing collection of pictures suitable for photogrammetric processing, but camera settings need to be carefully adjusted beforehand (O'Connor et al., 2017). If early morning flights are not feasible in the study area for logistical reasons or when surveying glaciers with eastern exposures, the latter scenario should be considered.

In terms of costs, UAV and terrestrial photogrammetric surveys are also advantageous, since TLS instruments are much more expensive at €70,000-100,000 compared to UAVs (€3500 for our

496 platform) and DSLR (Digital Single-Lens Reflex) cameras used in photogrammetry, in the €500-3500
497 range.

498 **6.4 Additional remarks**

499 In summary, although TLS point clouds are regarded as the most accurate (Naumann et al., 2013),
500 they suffer from inhomogeneous point density and cumbersome logistics, and their potential in glacial
501 environments is limited, unless a maximum uncertainty of 5-10 cm can be tolerated. Laser scanners
502 are also employed on aerial platforms, including UAVs, where they can reconstruct terrain
503 morphology with only slightly higher uncertainty than the terrestrial counterparts with a much greater
504 coverage (Raymond et al., 2009), but the high operational cost has limited the diffusion of this
505 technique. Lastly, photogrammetry from higher altitude aerial platforms (mostly planes, but also
506 helicopters and satellites) can similarly achieve low uncertainty (3 m, Andreassen et al., 2002) and
507 extensive coverage at the price of a lower spatial resolution compared to UAVs (e.g. 2 m in our case),
508 and due to its popularity in the past it is often the only means to acquire good quality archive data to
509 investigate glacier changes over broad time scales (Andreassen et al., 2002; Molg et al., 2017).

510 In our pilot study, we covered part of the Forni glacier tongue, and investigated different techniques
511 to map/monitor hazards related to the glacier collapse. Our maps can help identify safer paths where
512 mountaineers and skiers can visit the glacier and reach the most important summits. However, the
513 increase in collapse structures owing to climate change requires multi-temporal monitoring. A
514 comprehensive risk assessment should also cover the entire glacier, to investigate the probability of
515 serac detachment and provide an estimate of the glacier mass balance with the geodetic method. While
516 our integrated approach using a multicopter and terrestrial photogrammetry should be preferred to
517 TLS for the investigation of small individual ice bodies, fixed-wing UAVs, ideally equipped with an
518 RTK system and the ability to tilt the camera off-nadir, might be the platform of choice to cover large
519 distances (see e.g. Ryan et al., 2017), potentially reducing the number of flights and solving issues

with GCP placement. Such platforms could help collect sufficient data for hazard management strategies up to the basin scale in Stelvio National Park and other sectors of the Italian Alps, eventually replacing higher altitude aerial surveys. Cost analyses (Matese et al., 2015) should also be performed to evaluate the benefits of improved spatial resolution and lower DEM uncertainty of UAVs compared to aerial and satellite surveys and choose the best approach for individual cases.

7 Conclusions

In our study, we compared point clouds generated from UAV photogrammetry, close-range photogrammetry, and TLS to assess their quality and evaluate their potential in mapping and describing glacier hazards such as ring faults and normal faults, in a specific campaign carried out in summer 2016. In addition, we employed orthophotos and point clouds from a UAV survey conducted in 2014 to analyse the evolution of glacier hazards, as well as a DEM from an aerial photogrammetric survey conducted in 2007, to investigate glacier thickness changes between 2007 and 2016. The main findings of our study include:

- UAVs and terrestrial photogrammetric surveys provide reliable performances in glacial environments and outperform TLS in terms of logistics and costs.
- UAV and terrestrial photogrammetric blocks can be easily integrated providing more information than individual techniques to help identify glacier hazards.
- UAV-based DEMs can be employed to estimate thickness and volume changes but improvements are necessary in terms of area covered and to reduce uncertainty.
- The Forni Glacier is rapidly collapsing with an increase in ring fault sizes, providing evidence of climate change in the region.
- The glacier thinning rate increased owing to collapses to 5.20 ± 1.11 ma^{-1} between 2014 and 2016.

543 The maps produced from the combined analysis of UAV and terrestrial photogrammetric point clouds
544 and orthophotos can be made available through GIS web portals of the Stelvio National Park or the
545 Lombardy region (http://www.geoportale.regione.lombardia.it/). A permanent monitoring
546 programme should be set up to help manage risk in the area, issuing warnings and assisting mountain
547 guides in changing hiking and ski routes as needed. The analysis of glacier thickness changes suggests
548 a feedback mechanism which should be further analysed, with higher thinning rates leading to
549 increased occurrence of collapses. Glacier downwasting is also of relevance for risk management in
550 the protected area, providing valuable data to assess the increased chance of rockfalls and to improve
551 forecasts of glacier meltwater production.

552 While our test was conducted on one of the largest glaciers in the Italian Alps, the integrated
553 photogrammetric approach is easily transferable to similar sized and much smaller glaciers, where it
554 would be able to provide a comprehensive assessment of hazards and thickness changes and become
555 useful in decision support systems for natural hazard management. In larger regions, UAVs hold the
556 potential to become the platform of choice, but their performances and cost-effectiveness compared
557 to aerial and satellite surveys need to be further evaluated.

558 **Competing interests**

559 The authors declare that they have no conflict of interest.

560 **Acknowledgements**

561 This study was funded by DARAS, the Department for Autonomies and Regional Affairs of the Italian
562 government's Presidency of the Council of Ministers. The authors are grateful to the central scientific
563 committee of CAI (Club Alpino Italiano – Italian Alpine Club) and Levissima San Pellegrino S.P.A.
564 for funding the UAV quadcopter. The authors also thank Stelvio Park Authority for the logistic support
565 and for permitting the UAV surveys and IIT Regione Lombardia for the provision of the 2007 DEM.
566 Our gratitude also goes to the GICARUS lab of Politecnico Milano at Lecco Campus for providing

the survey equipment. Finally, the authors would also like to thank Tullio Feifer, Livio Piatta, and Andrea Grossoni for their help during field operations.

References

Abellán, A., Oppikofer, T., Jaboyedoff, M., Rosser, N. J., Lim, M. and Lato, M. J.: Terrestrial laser scanning of rock slope instabilities. Earth Surface Processes and Landforms, 39, 80–97, 2014, doi:10.1002/esp.3493.

Aicardi, I., Chiabrando, F.,Grasso, N., Lingua, A.M., Noardo, F. and Spanò, A.: UAV photogrammetry with oblique images: first analysis on data acquisition and processing, International Archives of the Photogrammetry, Remote Sensing and Spatial Information Sciences, Prague, Czech Republic, 12–19 July 2016, 41-B1, 835-842, 2016, doi: 10.5194/isprs-archives-XLI-B1-835-2016.

Andreassen, L.M., Hallgeir, E. and Kjollmoen, B.: Using aerial photography to study glacier changes in Norway, Annals of Glaciology, 34, 343-348, 2010, doi: 10.3189/172756402781817626

Azzoni, R.S., Fugazza, D., Zennaro, M., Zucali, M., D'Agata, C., Maragno, D., Cernuschi, M., Smiraglia, C. and Diolaiuti, G.A.: Recent structural evolution of Forni Glacier tongue (Ortles-Cevedale Group, Central Italian Alps). Journal of Maps, 13, 870-878, 2017, doi: 10.1080/17445647.2017.1394227

Berthier, E., Arnaud, Y., Kumar, R., Ahmad, S., Wagnon, P. and Chevallier, P.: Remote sensing estimates of glacier mass balances in the Himachal Pradesh (Western Himalaya, India), Remote Sensing of Environment, 108, 327-338, 2007, doi: 10.1016/j.rse.2006.11.017.

Berthier, E., Cabot, V., Vincent, C. and Six, D.: Decadal Region-Wide and Glacier-Wide Mass Balances Derived from Multi-Temporal ASTER Satellite Digital Elevation Models.Validation over the Mont-Blanc Area, Frontiers in Earth Science, 4, 63, 2016, doi: 10.3389/feart.2016.00063.

Bhardwaj, A., Sam, L., Akanksha, Martin-Torres, F.J. and Kumar, R.: UAVs as remote sensing platform in glaciology: Present applications and future prospects, Remote Sensing of Environment, 175, 196-204, 2016, doi: 10.1016/j.rse.2015.12.029.

Blasone, G., Cavalli, M. and Cazorzi, F.: Debris-Flow Monitoring and Geomorphic Change Detection Combining Laser Scanning and Fast Photogrammetric Surveys in the Moscardo Catchment (Eastern Italian Alps), in: Lollino, G., Arattano, M., Rinaldi, M., Giustolisi, O., Marechal, J.C. and Grant, G. (eds) Engineering Geology for Society and Territory, 3, Springer, Cham, 51-54, 2015, doi: 10.1007/978-3-319-09054-2_10.

Carey, M., McDowell, G., Huggel, C., Jackson, M., Portocarrero, C., Reynolds, J.M. and Vicuña, L.: Integrated approaches to adaptation and disaster risk reduction in dynamic sociocryospheric systems, in: Haeberli, W. and Whiteman, C. (Eds.), Snow and Ice-related Hazards, Risks and Disasters, Elsevier, 219-261, 2014, doi: 10.1016/B978-0-12-394849-6.00008-1.

Chandler, J.H. and Buckley, S.: Structure from motion (SFM) photogrammetry vs terrestrial laser scanning. In: Carpenter, M.B. and Keane, C.M. (eds.) Geoscience Handbook 2016, AGI Data Sheets, 5th ed. Alexandria, US, American Geosciences Institute, Section 20.1, 2016.

605 Chiarle, M., Iannotti, S., Mortara, G. and Deline, P.: Recent debris flow occurrences associated with
606 glaciers in the Alps, Global and Planetary Change, 56, 123-136, 2007, doi:
607 10.1016/j.gloplacha.2006.07.003.

608 Clague, J.: Glacier Hazards, in: Bobrowski, P. (Ed.), Encyclopedia of Natural Hazards, Springer,
609 400-405, 2013, doi: 10.1007/978-1-4020-4399-4_156.

610 Colomina, I. and Molina, P.: Unmanned aerial systems for photogrammetry and remote sensing: A
611 review, ISPRS Journal of Photogrammetry and Remote Sensing, 92, 79-97, 2014, doi:
612 10.1016/j.isprsjprs.2014.02.013.

613 D'Agata, C., Bocchiola, D., Maragno, D., Smiraglia, C. and Diolaiuti, G.A.: Glacier shrinkage
614 driven by climate change during half a century (1954–2007) in the Ortles-Cevedale group (Stelvio
615 National Park, Lombardy, Italian Alps), Theoretical and Applied Cimatology, 116, 169-190, 2014,
616 doi: 10.1007/s00704-013-0938-5.

617 Dall'Asta, E., Thoeni, K., Santise, M., Forlani, G., Giacomini, A., Roncella, R.: Network design and
618 quality checks in automatic orientation of close-range photogrammetric blocks, Sensors, 15, 7985-
619 8008, 2015, doi: 10.3390/s150407985

620 Dewez, T.J.B., Leroux, J. and Morelli, S.: Cliff collapse hazard from repeated multicopter UAV
621 acquisitions: return on experience, The International Archives of the Photogrammetry, Remote
622 Sensing and Spatial Information Sciences, XXIII ISPRS Congress, Prague, Czech Republic, 12–19
623 July 2016, 41-B5, 805-811, 2016, doi: 10.5194/isprs-archives-XLI-B5-805-2016

624 Diolaiuti, G.A. and Smiraglia, C.: Changing glaciers in a changing climate: how vanishing
625 geomorphosites have been driving deep changes in mountain landscapes and environments,
626 Géomorphologie : Relief, Processus, Environnement, 2, 131-152, 2010, doi:
627 10.4000/geomorphologie.7882.

628 Diolaiuti, G.A., Bocchiola, D., D'Agata, C. and Smiraglia, C.: Evidence of climate change impact
629 upon glaciers' recession within the Italian Alps, Theoretical and Applied Climatology, 109,429-445,
630 2012, doi: 10.1007/s00704-012-0589-y

631 Eltner, A., Kaiser, A., Castillo, C., Rock, G., Neugirg, F. and Abellán, A.: Image-based surface
632 reconstruction in geomorphometry – merits, limits and developments. Earth Surface Dynamics, 4,
633 359-389, 2016, doi: 10.5194/esurf-4-359-2016.

634 Fey, C. and Wichmann, V.: Long-range Terrestrial laser scanning for geomorphological change
635 detection in alpine terrain - handling uncertainties. Earth Surface Processes and Landforms, 42,
636 789-802, 2016, doi: 10.1002/esp.4022.

637 Fischer, M., Huss, M., Barboux, C. and Hoelzle, M.: The new Swiss Glacier Inventory SGI2010:
638 relevance of using high-resolution source data in areas dominated by very small glaciers, Arctic,
639 Antarctic and Alpine Research, 46,933-945, 2014, doi: 10.1657/1938-4246-46.4.933.

640 Fischer, M., Huss, M. and Hoelzle, M.: Surface elevation and mass changes of all Swiss glaciers
641 1980–2010, The Cryosphere, 9, 525-540, 2015, doi: 10.5194/tc-9-525-2015

642 Forlani, G., Pinto, L., Roncella, R. and Pagliari, D.: Terrestrial photogrammetry without ground
643 control points, Earth Science Informatics, 7, 71-81, 2014, doi: 10.1007/s12145-013-0127-1.

644 Fugazza, D., Senese, A., Azzoni, R.S., Smiraglia, C., Cernuschi, M., Severi, D. and Diolaiuti, G.A.:
645 High-resolution mapping of glacier surface features. The UAV survey of the Forni glacier (Stelvio
646 national park, Italy), Geografia Fisica e Dinamica Quaternaria, 38, 25-33, 2015, doi:
647 10.4461/GFDQ.2015.38.03.

648 Garavaglia, V., Diolaiuti, G.A., Smiraglia, C., Pasquale, V. and Pelfini, M.: Evaluating Tourist
649 Perception of Environmental Changes as a Contribution to Managing Natural Resources in
650 Glacierized areas: A Case Study of the Forni Glacier (Stelvio National Park, Italian Alps),
651 Environmental Management, 50, 1125-1138, 2012, doi: 10.1007/s00267-012-9948-9.

652 Gagliardini, O., Gillet-Chaulet, F., Durand, G., Vincent, C. and Duval, P.: Estimating the risk of
653 glacier cavity collapse during artificial drainage: The case of Tête Rousse Glacier, Geophysical
654 Research Letters, 38, L10505, 2011, doi:10.1029/2011GL047536.

655 Gardent, M., Rabatel, A., Dedieu, J.-P., Deline, P.: Multitemporal glacier inventory of the French Alps
656 from the late 1960s to the late 2000s, Global and Planetary Change, 120, 24-37, 2014. doi:
657 10.1016/j.gloplacha.2014.05.004.

658 Gindraux, S., Boesch, R. and Farinotti, D.: Accuracy Assessment of Digital Surface Models from
659 Unmanned Aerial Vehicles' Imagery on Glaciers, Remote sensing, 9, 186, 2-15, 2017,
660 doi:10.3390/rs9020186.

661 Gobiet, A., Kotlarski, S., Beniston, M., Heinrich, G., Rajczak, J., Stoffel, M.: 21st century climate
662 change in the European Alps—A review, Science of The Total Environment, 493, 1138-1151, 2014,
663 doi: 10.1016/j.scitotenv.2013.07.050.

664 Harris, C., Arenson, L.U., Christiansen, H.H., Etzelmueller, B., Frauenfelder, R., Gruber, S., Haeberli,
665 W., Hauck, C., Hoelzle, M., Humlum, O., Isaksen, K., Kaab, A., Kern-Luetschg, M., Lehning, M.,
666 Matsuoka, N., Murton, J.B., Noetzli, J., Phillips, M., Ross, N., Seppaelae, M., Springman, S.M. and
667 Vonder Muehll, D.: Permafrost and climate in Europe: Monitoring and modelling thermal,
668 geomorphological and geotechnical responses, Earth-Science Reviews, 92, 117-171, 2009, doi:
669 10.1016/j.earscirev.2008.12.002.

670 Hoffmann-Wellenhof, B., Lichtenegger, H. and Wasle, E.: GNSS – GPS, GLONASS, Galileo & more,
671 Springer, 2008, doi: 10.1007/978-3-211-73017-1.

672 Immerzeel, W.W., Kraaijenbrink, P.D.A., Shea, J.M., Shrestha, A.B., Pellicciotti, F., Bierkens, M.F.P.
673 and de Jong, S.M.: High-resolution monitoring of Himalayan glacier dynamics using unmanned aerial
674 vehicles, Remote Sensing of Environment, 150,93-103, 2014, doi: 10.1016/j.rse.2014.04.025.

675 Janke, J.R.: Using airborne LiDAR and USGS DEM data for assessing rock glaciers and glaciers,
676 Geomorphology, 195, 118-130, doi: 10.1016/j.geomorph.2013.04.036

677 Jokinen, O. and Geist T.: Accuracy aspects in topographical change detection of glacier surface, in:
678 Remote sensing of glaciers, CRC Press/Balkema, Leiden, the Netherlands, 269-283, 2010, doi:
679 10.1201/b10155-15.

680 Kaab, A., Huggel., C., Fischer, L., Guex, S. Paul, F., Roer., I., Salzmann, N., Schlaefli, S., Schmutz,
681 K., Schneider, D., Strozzi, T. and Weidmann, Y.: Remote sensing of glacier- and permafrost-related
682 hazards in high mountains: an overview, Natural Hazards and Earth System Sciences, 5, 527–554,
683 2005a, doi: 10.5194/nhess-5-527-2005.

Kaab, A., Reynolds, J.M. and Haeberli, W.: Glacier and Permafrost hazards in high mountains, in: Huber U.M., Bugmann H.K.M., Reasoner M.A. (eds) Global Change and Mountain Regions. Advances in Global Change Research, Springer, Dordrecht, 225-234, 2005b, doi: 10.1007/1-4020-3508-X_23.

Kaufmann, V. and Ladstädter, R.: Application of terrestrial photogrammetry for glacier monitoring in Alpine environments, International Archives of the Photogrammetry, Remote Sensing and Spatial Information Sciences, Beijing, China, 37-B8, 813-818, 2008.

Kaufmann, V. and Seier, G.: Long-term monitoring of glacier change at Gössnitzkees (Austria) using terrestrial photogrammetry, The International Archives of the Photogrammetry, Remote Sensing and Spatial Information Sciences, XXIII ISPRS Congress, Prague, Czech Republic, 12-19 July 2016, 41-B8, 495-502, 2016, doi: 10.5194/isprs-archives-XLI-B8-495-2016

Keiler, M., Knight, J. and Harrison, S.: Climate change and geomorphological hazards in the eastern European Alps, Philosophical Transactions of The Royal Society A, 368, 2461–2479, 2010, doi: 10.1098/rsta.2010.0047.

Kellerer-Pirklbauer, A., Bauer, A. and Proske, H.: Terrestrial laser scanning for glacier monitoring: Glaciation changes of the Gößnitzkees glacier (Schober group, Austria) between 2000 and 2004, 3rd Symposion of the Hohe Tauern National Park for research in protected areas, castle of Kaprun, Austria, 15-17 September 2005, 97-106, 2005.

Lague, D., Brodu, N., Leroux, J.: Accurate 3D comparison of complex topography with terrestrial laser scanner: application to the Rangitikei canyon (N-Z). Journal of Photogrammetry and Remote Sensing, 82, 10–26, 2013, doi:10.1016/j.isprsjprs.2013.04.009.

Matese, A., Toscano, P., Di Gennaro, S.F., Genesio, L., Vaccari, F.P., Primicerio, J., Belli, C., Zaldei, A., Bianconi, R., Gioli, B.: Intercomparison of UAV, Aircraft and Satellite Remote Sensing Platforms for Precision Viticulture, Remote Sensing, 7, 2971-2990, 2015, doi:10.3390/rs70302971.

Moelg, N. and Bolch, T.: Structure-from-Motion Using Historical Aerial Images to Analyse Changes in Glacier Surface Elevation, Remote Sensing, 9, 1021, 2017, doi:10.3390/rs9101021

Naumann, M., Geist, M., Bill, R., Niemeyer, F. and Grenzdoerffer, G.: Accuracy comparison of digital surface models created by Unmanned Aerial Systems imagery and Terrestrial Laser Scanner, International Archives of the Photogrammetry, Remote Sensing and Spatial Information Sciences, UAV-g2013, 4-6 September 2013, Rostock, Germany, 61-W2, 281-286, 2013, doi: 10.5194/isprsarchives-XL-1-W2-281-2013

Nuth, C. and Kaab, A.: Co-registration and bias corrections of satellite elevation data sets for quantifying glacier thickness change, The Cryosphere, 5, 271-290, 2011, doi: 10.5194/tc-5-271-2011.

Oborne, M.: Mission planner software. Available at: http://ardupilot.org/planner/, last access: 18/05/2017, 2013.

O'Connor, J., Smith, M.J. and James, M.R.: Cameras and settings for aerial surveys in the geosciences: optimising image data, Progress in Physical Geography, 41, 1-20, 2017, doi: 10.1177/0309133317703092.

722 Palomo, I.: Climate Change Impacts on Ecosystem Services in High Mountain Areas: A Literature
723 Review, Mountain Research and Development, 37,179-187, 2017, doi: 10.1659/MRD-JOURNAL-
724 D-16-00110.1.

725 Piermattei, L., Carturan, L. and Guarnieri, A.: Use of terrestrial photogrammetry based on structure
726 from motion for mass balance estimation of a small glacier in the Italian Alps. Earth Surface
727 Processes and Landforms, 40, 1791-1802, 2015, doi: 10.1002/esp.3756.

728 Piermattei, L., Carturan, L., de Blasi, F., Tarolli, P., Dalla Fontana, G., Vettore, A. and Pfeifer, N.:
729 Suitability of ground-based SfM–MVS for monitoring glacial and periglacial processes, Earth
730 Surface Dynamics, 4, 325-443, 2016, doi: 10.5194/esurf-4-425-2016.

731 Pomerleau, F., Colas, F., Siegwart, R. and Magnenat, S.: Comparing ICP variants on real world data
732 sets. Autonomous Robots, 34, 133–148, 2013, doi: 10.1007/s10514-013-9327-2.

733 Quincey, D.J., Lucas, R.M., Richardson. S.D., Glasser, N.F., Hambrey, N.J. and Reynolds, J.M.:
734 Optical remote sensing techniques in high-mountain environments: application to glacial hazards,
735 Progress in Physical Geography, 29, 475-505, 2005, doi: 10.1191/0309133305pp456ra.

736 Rayburg, S., Thoms, M. and Neave, M.: A comparison of digital elevation models generated from
737 different data sources, Geomorphology, 106, 261-270, 2009, doi: 10.1016/j.geomorph.2008.11.007

738 Riccardi, A., Vassena, G., Scotti, R., Sgrenzaroli, M.: Recent evolution of the punta S.Matteo serac
739 (Ortles-Cevedale Group, Italian Alps), Geografia Fisica e Dinamica Quaternaria, 33, 215-219, 2010.

740 Rolstad, C., Haug, T. and Denby, B.: Spatially integrated geodetic glacier mass balance and its
741 uncertainty based on geostatistical analysis: application to the western Svartisen ice cap, Norway,
742 Journal of Glaciology, 55, 666-680, 2009, doi: 10.3189/172756409787769528

743 Rounce, D.R., Watson, C.S. and McKinney, D.C.: Identification of Hazard and Risk for Glacial Lakes
744 in the Nepal Himalaya Using Satellite Imagery from 2000–2015, Remote Sensing, 9, 654, 2017,
745 doi:10.3390/rs9070654.

746 Ryan, J.C., Hubbard, A., Box, J.E., Brough, S., Cameron, K., Cook, J.M., Cooper, M., Doyle, S.H.,
747 Edwards, A., Holt, T., Irvine-Fynn, T., Jones, C., Pitcher, L.H., Rennermalm, A.K., Smith, L.C, Stibal,
748 M. and Snooke, N.: Derivation of High Spatial Resolution Albedo from UAV Digital Imagery:
749 Application over the Greenland Ice Sheet, Frontiers in Earth Science, 5, 40, 2017, doi:
750 10.3389/feart.2017.00040.

751 Seier, G., Kellerer-Pirklbauer, A., Wecht, M., Hirschmann, S., Kaufmann, V., Lieb, G.K. and Sulzer,
752 W.: UAS-Based Change Detection of the Glacial and Proglacial Transition Zone at Pasterze Glacier,
753 Austria. Remote Sensing, 9, 549, 2017, doi:10.3390/rs9060549.

754 Senese, A., Diolaiuti, G.A., Mihalcea, C. and Smiraglia, C.: Energy and Mass Balance of Forni
755 Glacier (Stelvio National Park, Italian Alps) from a Four-Year Meteorological Data Record, Arctic,
756 Antarctic and Alpine Research, 44, 122-134, 2012, doi: 10.1657/1938-4246-44.1.122.

757 Smiraglia, C., Azzoni, R.S., D'Agata, C., Maragno, D., Fugazza, D. and Diolaiuti, G.A.: The
758 evolution of the Italian glaciers from the previous data base to the new Italian inventory. Preliminary
759 considerations and results, Geogr. Fis. Dinam. Quat., 38, 79-87, 2015, doi:
760 10.4461/GFDQ.2015.38.08.

761 Teunissen, P.J.G.: Testing theory. An introduction. Series on Mathematical Geodesy and Positioning,
762 VSSD Delft, The Netherlands, 2009.

763 Urbini, S., Zirizzotti, A., Baskaradas, J.A., Tabacco, I.E., Cafarella, L., Senese, A., Smiraglia, C.,
764 Diolaiuti, G.: Airborne radio echo sounding (RES) measures on alpine glaciers to evaluate ice
765 thickness and bedrock geometry: Preliminary results from pilot tests performed in the ortles-cevedale
766 group (Italian alps), Annals of Geophysics, 60, G0226, doi: 10.4401/ag-7122, 2017.

767 Vincent, C., Auclair, S. and Le Meur, E.: Outburst flood hazard for glacier-dammed Lac de
768 Rochemelon, France, Journal of Glaciology, 56, 91-100, 2010, doi: 10.3189/002214310791190857

769 Vincent, C., Thibert, E., Harter, M., Soruco, A. and Gilbert, A.: Volume and frequency of ice
770 avalanches from Taconnaz hanging glacier, French Alps, Annals of Glaciology, 56, 17-25, 2015, doi:
771 10.3189/2015AoG70A017.

772 Westoby, M.J., Brasington, J., Glasser, N.F., Hambrey, M.J. and Reynolds, J.M.: Structure-from-
773 Motion' photogrammetry: A low-cost, effective tool for geoscience applications, Geomorphology,
774 179, 300-314, 2012, doi: 10.1016/j.geomorph.2012.08.021.

775 Winkler, M., Pfeffer, W.T. and Hanke, K.: Kilimanjaro ice cliff monitoring with close range
776 photogrammetry, International Archives of the Photogrammetry, Remote Sensing and Spatial
777 Information Sciences, XXII ISPRS Congress, Melbourne, Australia, 25 August-1 September 2012,
778 39-B5, 441-446, 2012.

779

Tables

DEM pair	Elevation differences without co-registration shifts ($\mu_{\Delta H}\pm\sigma_{\Delta H}$) [m]	Co-registration shifts		Elevation differences with co-registration shifts ($\mu_{\Delta H}\pm\sigma_{\Delta H}$) [m]
		X [m]	Y [m]	
2007-2014	1.96±2.60	1.11	-1.11	0.00±1.70
2007-2016	-0.43±3.48	2.44	-1.11	0.00±2.60
2014-2016	-2.92±3.21	-0.20	-1.30	0.00±2.22

Table 1: Statistics of the elevation differences between DEM pairs before and after the application of co-registration shifts. DEM 2007 from aerial multispectral survey, DEM 2014 and DEM 2016 from UAV photogrammetry.

Sample Window	Area (m^2)	Number of points in sample windows			Mean and standard deviation of point density [points/m^2]			Number of points above the lower 12.5% percentile		
		UAV	TP	TLS	UAV	TP.	TLS	UAV	TP	TLS
1	2793	-	1984k	141k	-	1654±637	226±100	-	880	26
2	1806	76k	2175k	130k	109±29	2297±708	391±217	61	881	0
3	495	43k	712k	25k	103±27	1978±606	151±60	49	766	31
4	672	62k	557k	33k	108±22	1384±530	141±69	62	324	2
5	3960	406k	810k	-	141±22	485±227	-	97	31	-

Table 2: Area and number of points in each sample window on the Forni Glacier terminus, mean and standard deviation of local point density and number of points above the lower 12.5% percentile in each window. k stands for thousands of points. UAV refers to UAV photogrammetry, TP to terrestrial photogrammetry and TLS to terrestrial laser scanning.

Sample Window		Means and Std. Dev.s of M3C2 distances [cm]			RMSE of M3C2 distances [cm]		
	Ref.	TLS	TLS	UAV	TLS	TLS	UAV
	Slave	TP	UAV	TP	TP	UAV	TP
1		4.5±7.4	-	-	8.7	-	-
2		-1.1±10.5	14.8±34.7	-14.5±26.7	10.6	37.7	30.4
3		8.4±4.1	14.7±15.1	-8.5±18.9	9.4	21.1	20.7
4		2.8±5.3	9.4±22.2	-2.3±24.9	6.0	24.0	25.0
5		-	-	-8.5±25.3	-	-	26.7

Table 3: Statistics on distances between point clouds computed on the basis of the M3C2 algorithm, showing mean, standard deviation and root mean square error (RMSE) of each point cloud pair. UAV refers to UAV photogrammetry, TP to terrestrial photogrammetry and TLS to terrestrial laser scanning. Ref. stands for reference and "-" means no comparison was performed.

DEM pair	Mean thickness change [m]	Mean thinning rates [ma^{-1}]	Volume Change [10^6 m^3]
2007-2014	-31.91 ± 1.70	-4.55 ± 0.24	-10.00 ± 0.17 (1.74%)
2007-2016	-42.86 ± 2.60	-4.76 ± 0.29	-13.46 ± 0.20 (1.47%)
2014-2016	-10.41 ± 2.22	-5.20 ± 1.11	-3.29 ± 0.08 (2.60%)

799 *Table 4: Average ice thickness change, thinning rates and volume loss from DEM differencing over a common*
800 *reference area of 0.32 km^2 for all DEM pairs. Uncertainty of thickness change expressed as one standard*
801 *deviation of residual elevation differences over stable areas after DEM co-registration.*

802

Figures

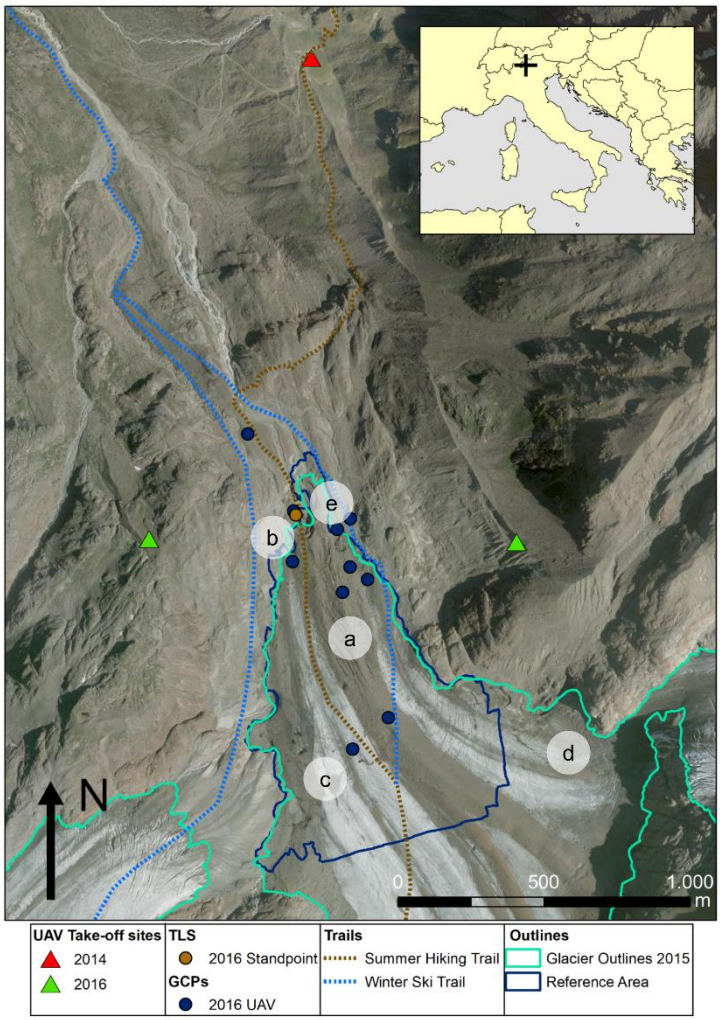

Figure 1: the tongue of Forni Glacier. The map shows the location of take-off/landing sites for the 2014 and 2016 UAV surveys, standpoint of TLS survey, GCPs used in the UAV photogrammetry surveys and trails crossing the glaciers. Letters a-e identify the location of features described in Fig.2. Base map from 2015 courtesy of IIT Regione Lombardia WMS Service. Trails from Kompass online cartography at https://www.kompass-1039 italia.it/info/mappa-online/..

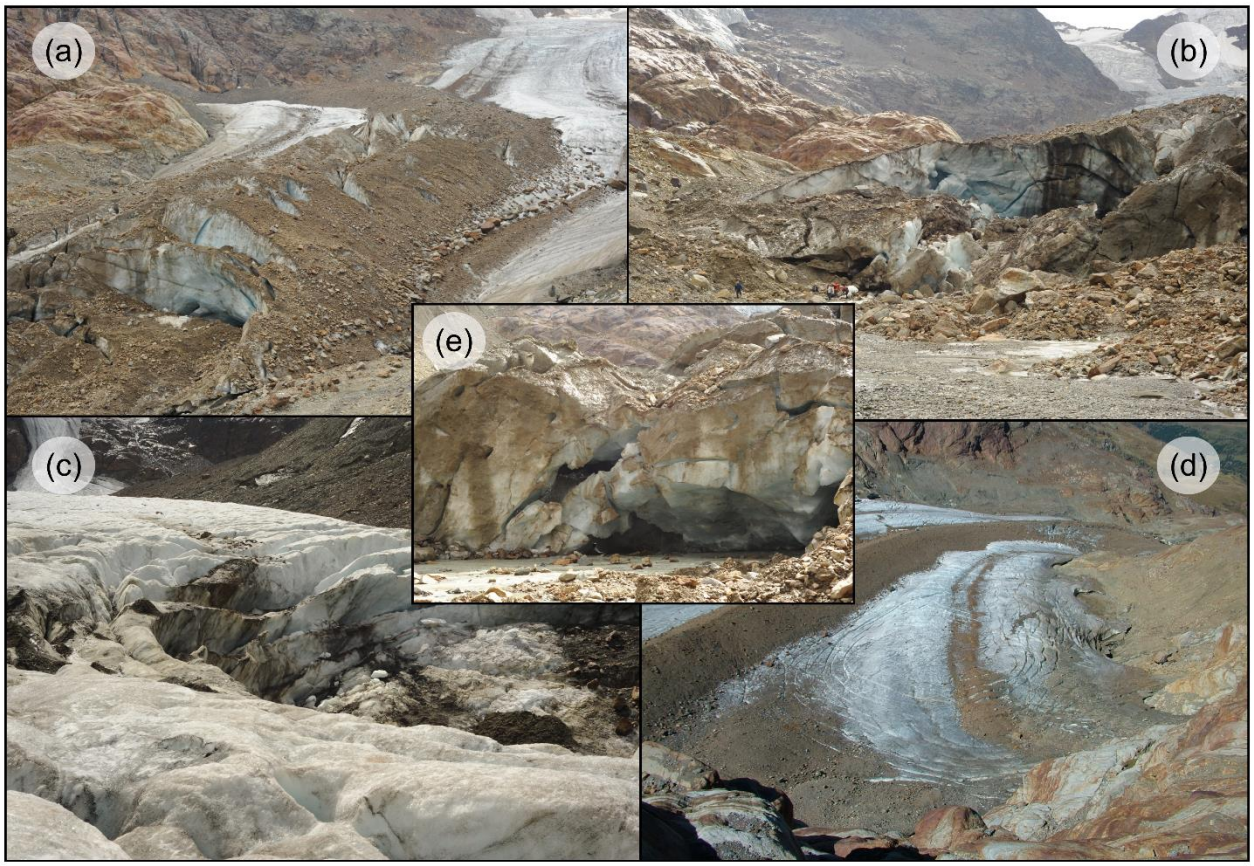

Figure 2: Collapsing areas on the tongue of Forni Glacier. (a) Faults cutting across the eastern medial moraine; (b) glacier terminus; (c) Near-circular collapsed area on the central tongue; (d) Large ring fault on the eastern tongue at the base of the icefall. Photo courtesy of G.Cola; (e) Close-up of a vertical ice cliff at the glacier terminus. The location of features is reported in Fig.1

Aircraft type	Swinglet CAM, Commercial platform
Digital Camera	Canon Ixus 127 HS
Camera technical features	16 Megapixel, focal length 4.3 mm
GNSS antenna	GPS only
Weight (incl. payload)	0.50 Kg
Battery time	30 minutes

Aircraft type	Customized, with Tarot frame 650 size, VR Brain 5.2 Autopilot & APM Arducopter 3.2.1 Firmware
Digital camera	Canon Powershot ELPH 320 HS
Camera technical features	16 Megapixel, focal length 4.3 mm
GNSS antenna	GPS+GLONASS (Galileo compatible)
Weight (incl. payload)	2.75 Kg
Battery time	20-25 minutes

820

821 *Figure 3: The UAVs used in surveys of the Forni Glacier and their characteristics. (a) The SwingletCam fixed-*
822 *wing aircraft employed in 2014, at its take off site by Lake Rosole; (b) The customized quadcopter used in*
823 *2016 in the lab.*

824

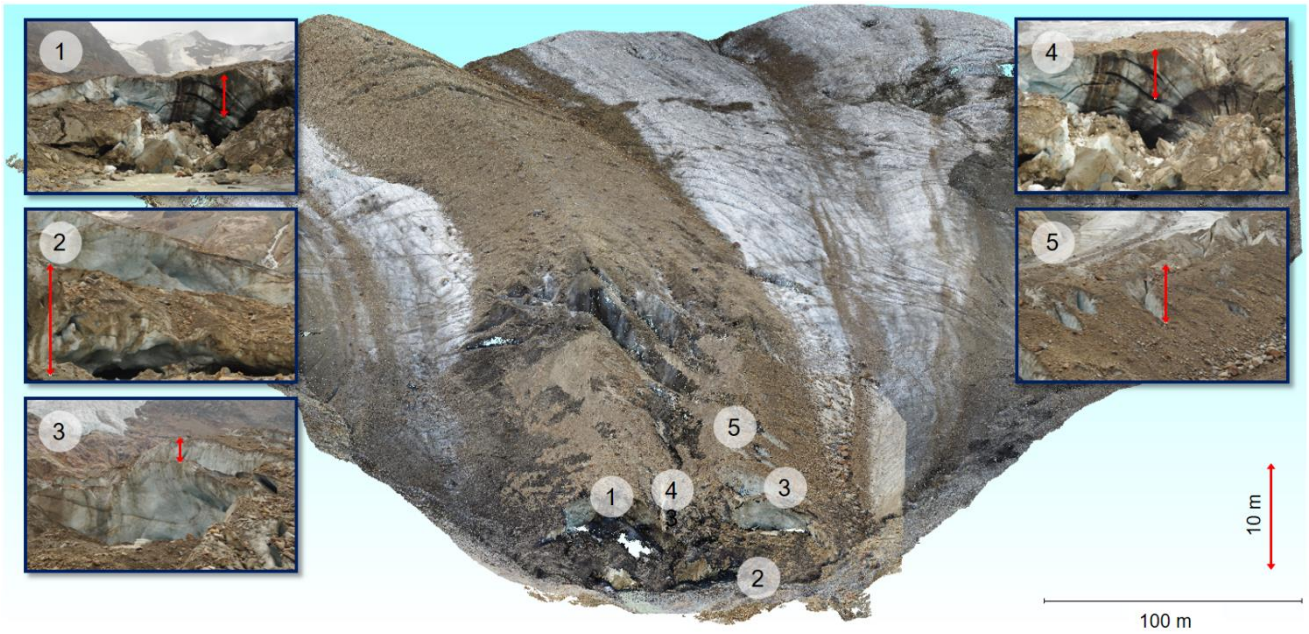

Figure 4: Location of different glacier features or hazard-prone areas on the tongue of Forni glacier were the point cloud comparison was performed. The background image is the merged point cloud generated from the 2016 UAV and terrestrial photogrammetry survey.

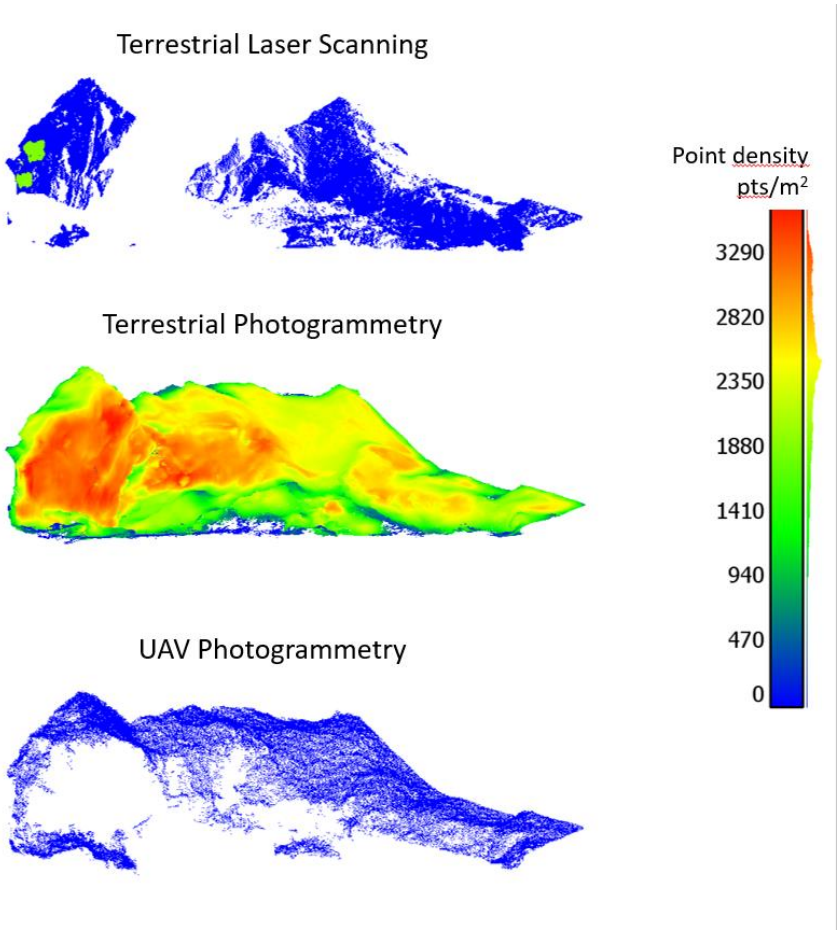

Figure 5: Maps of point density in sample location 2.

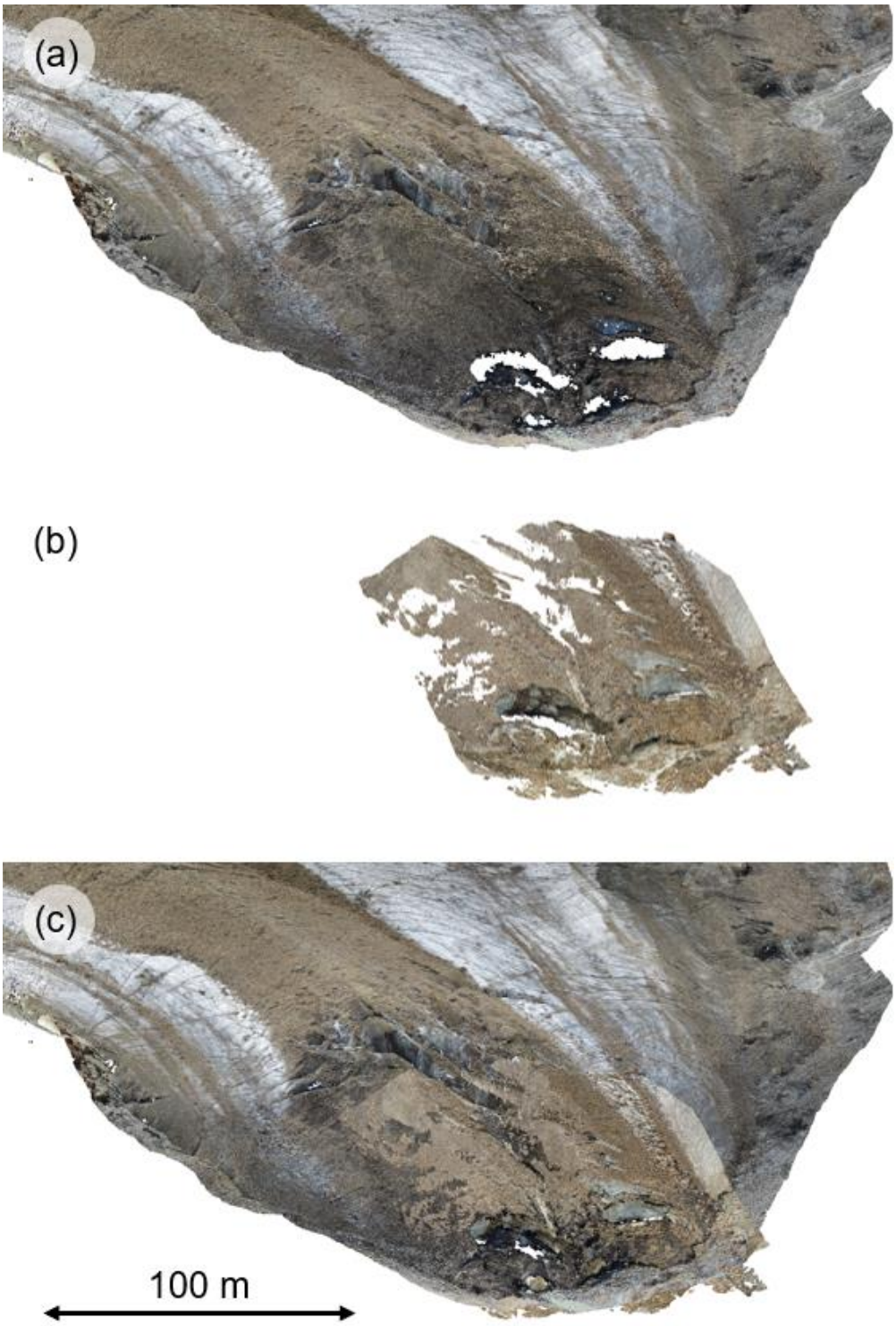

Figure 6: Spatial coverage of UAV- and terrestrial photogrammetry point clouds and merged point cloud from the two techniques. a) UAV photogrammetry point cloud; b) terrestrial photogrammetry point cloud; c) merged point cloud.

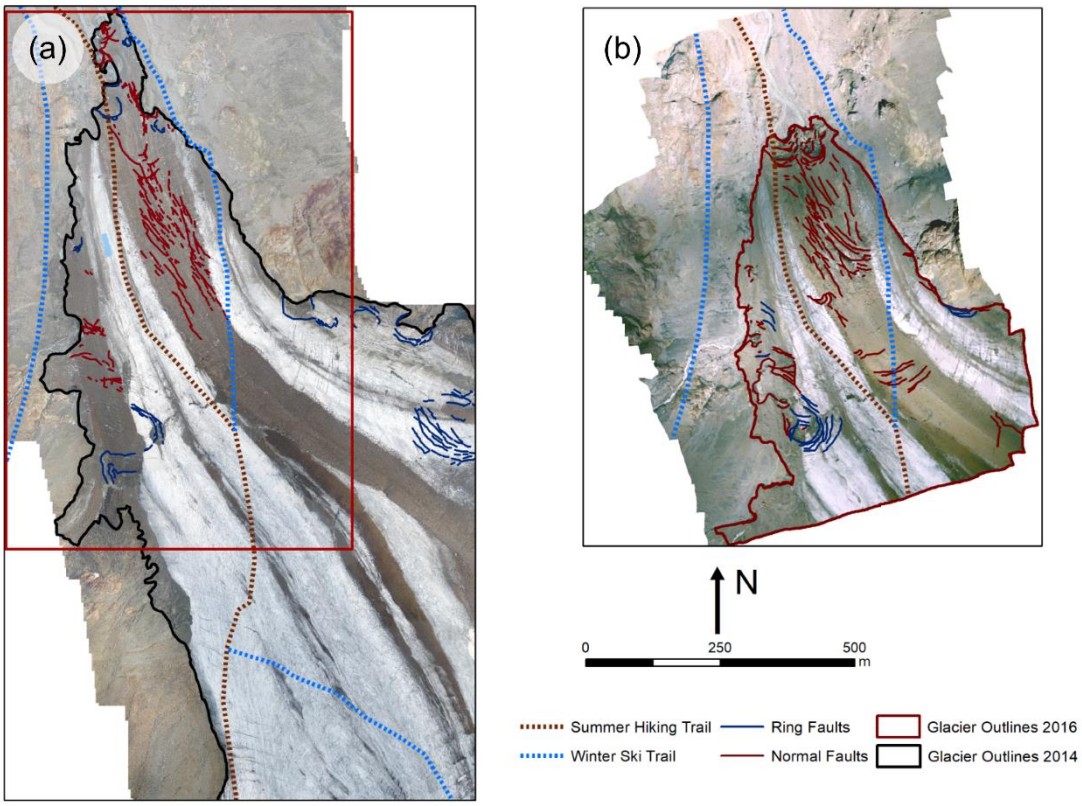

837

838 *Figure 7: Location of collapse structures, i.e. normal faults and ring faults and trails crossing the*
839 *Forni Glacier. (a) Collapse structures in 2014, with 2014 UAV ortophoto as basemap. The red box*
840 *marks the area surveyed in 2016. (b) Collapse structures in 2016, with 2016 UAV orthophoto as*
841 *basemap. Trails from Kompass online cartography at https://www.kompass-*1039 *italia.it/info/mappa-*
842 *online/.*

843

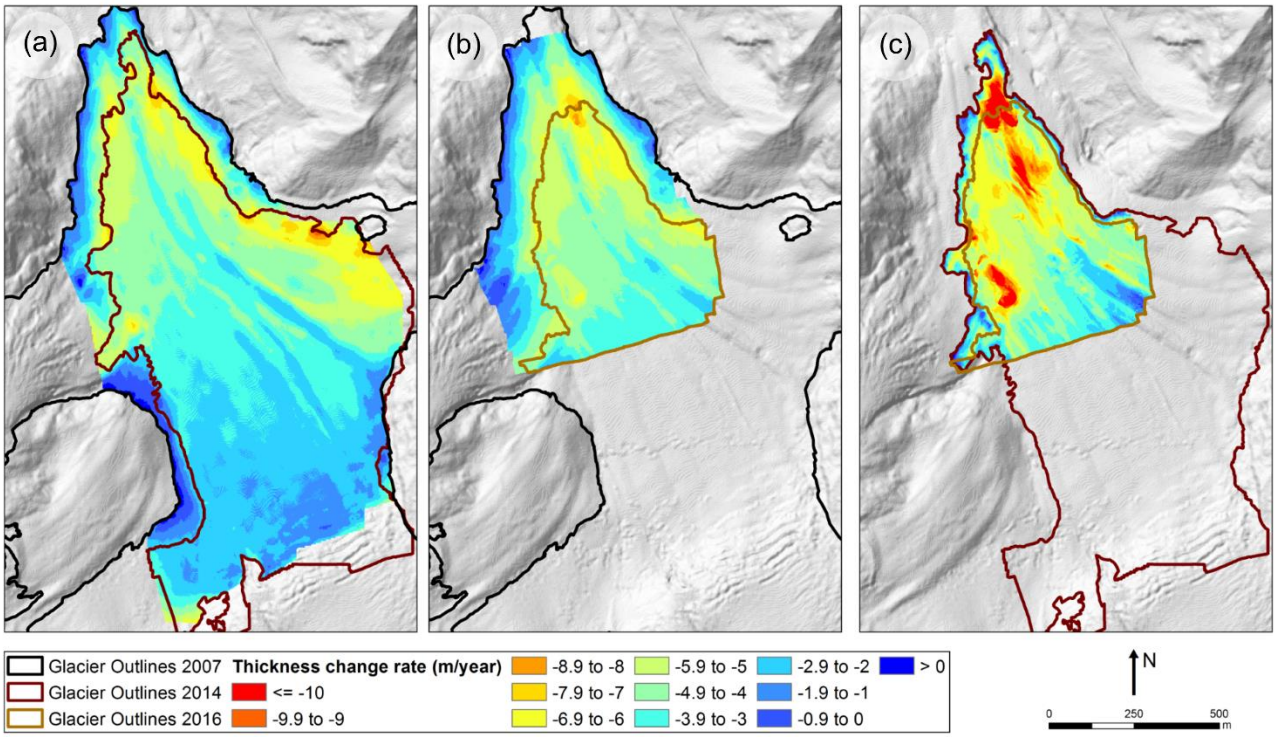

844
845 *Figure 8: Ice thickness change rates from DEM differencing over (a) 2007-2014; (b) 2007-2016; (c)*

846 *2014-2016. Glacier outlines from 2014 and 2016 are limited to the area surveyed during the UAV*

847 *campaigns. Base map from hillshading of 2007 DEM.*

848

849
850